19th Brazilian Congress of Thermal Sciences and Engineering
November 06th-10th, 2022, Bento Gonçalves - RS - Brazil

ENC-2022-0470
NUMERICAL COMPARISON ON THERMAL PERFORMANCE OF DIFFERENT CROSS SECTIONS OF PIN-FIN HEAT SINKS

Rafael San Martin Moreira
Luz E. Peñaranda Chenche
Diego Busson de Moraes
Carolina P. Naveira-Cotta
Federal University of Rio de Janeiro, Laboratory of Nano, Microfluidics and Microsystems - LabMEMS, Mechanical Eng. Dept., POLI & COPPE/UFRJ, Rio de Janeiro/RJ, Brazil
rafaelsanmartin@mecanica.coppe.ufrj.br, ing.elenap@gmail.com, bussonn@gmail.com, carolina@mecanica.coppe.ufrj.br

Paulo Roberto Siqueira da Costa Júnior
Wikki Brasil LTDA, Technological Park, Federal University of Rio de Janeiro, Rio de Janeiro, RJ, Brazil
paulorobertoscj@gmail.com

João A. Lima[1,2]
[1] Federal University of Rio de Janeiro, Laboratory of Nano, Microfluidics and Microsystems - LabMEMS, Mechanical Eng. Dept., POLI & COPPE/UFRJ, Rio de Janeiro/RJ, Brazil
[2] Renewable Energy Eng. Dept., CEAR - Federal University of Paraíba, João Pessoa/PB, Brazil
jalima@cear.ufpb.br

Abstract. *Recently, due to the grown development of micro devices in different fields of applications such as electronics, solar, bio engineering, etc., the needing of more efficient of heating removal sink has become an essential concern in this field of science. In this sense, pin fin configuration has been shown high cooling capacity and assists in uniform temperature distribution with a low pressure drop. In this context, this work aims to analyze four different pin-fin geometries (diamond, drop, sinusoidal, and circular), in the staggered configuration, in the search for the best thermohydraulic performance in microscale heat exchangers, which will be attached to solar cells installed in a high-concentration photovoltaic system (HCPV). The geometries were obtained through DLMM (direct laser metal melting) additive manufacturing process, satisfying the required dimensional quality. It was constated that the construction of channels with pin fins proved to be more effective in terms of heat exchange when compared to straight microchannels with rectangular cross section results, without compromising to much the pumping power needed for the fluid flow. Additionally, it was also be observed that the sine, drop and diamond shapes presented results with higher fluid outlet temperature and a smaller pressure drop results than the microchannel. Among these three pin-fin geometric models, the droplet model produced the highest heat exchanges, resulting in the highest enthalpic gain by the fluid at the HCPV exchanger outlet.*

Keywords: *Pin fin, Numerical Simulation, Micro Heat Sink, Thermal Performance*

1. INTRODUCTION

In recent years, new geometries have been proposed for microscale heat exchangers, mainly aiming to achieve increases in heat exchange efficiency, but without greatly penalizing the pressure drop of the device, an effect commonly observed in a large number of studies. In this sense, “pin fins” forest heatsink configurations have been shown to be a viable solution in the pursuit of this objective (AlFalah et al., 2022; Cohen & Bourell, 2016; Radmard et al., 2021; Tang et al., 2022; Yang et al., 2017).

The pin fin configuration presents high cooling capacity and assists in uniform temperature distribution with a low pressure drop. For this reason, different pin-fin geometries have been studied, such as hydrofoil, sine, rectangular, elliptical, diamond, circular, etc., but without a consensus on the type of pin that allows achieving better thermo-hydraulic performance values in microscale heat exchangers. The type of pin morphology and dimensions play the role on the pin-fin efficiency, and in particular, the spacing characteristic between pins is a very important parameter.

On the other hand, one of the main limitations for application of this type of geometric configuration is that traditional manufacturing techniques such as extrusion (Morrison, 2002), micro electric discharge machining (Wang et al., 2005) and milling (Baisar & Briggs, 2009), still present great difficulty in achieving dimensional design compliance. Therefore, additive manufacturing processes have emerged as an alternative for manufacturing of pin fin dies (Cohen & Bourell, 2016; Klein et al., 2018; Tsopanos et al., 2006), and it has been demonstrated that, depending on the morphology, dimensions and spacing values used, dimensional quality can be achieved in the manufactured parts.

According to the literature (Ali & Arshad, 2015; Mohammadi & Koşar, 2019; Roth et al., 2013; Yan et al., 2021) that point out that the staggered pin configuration offers better performance characteristics of heat transfer, and based on preliminary analysis of microscopy images for evaluation of dimensional quality, the morphologies that showed greater compatibility in the manufacturing process were chosen for computational simulation, namely, the diamond, drop, sinusoidal, and circle geometries. Fig. 1 illustrates schematic sketches of the main geometric characteristics of the selected pin-fins shapes studied.

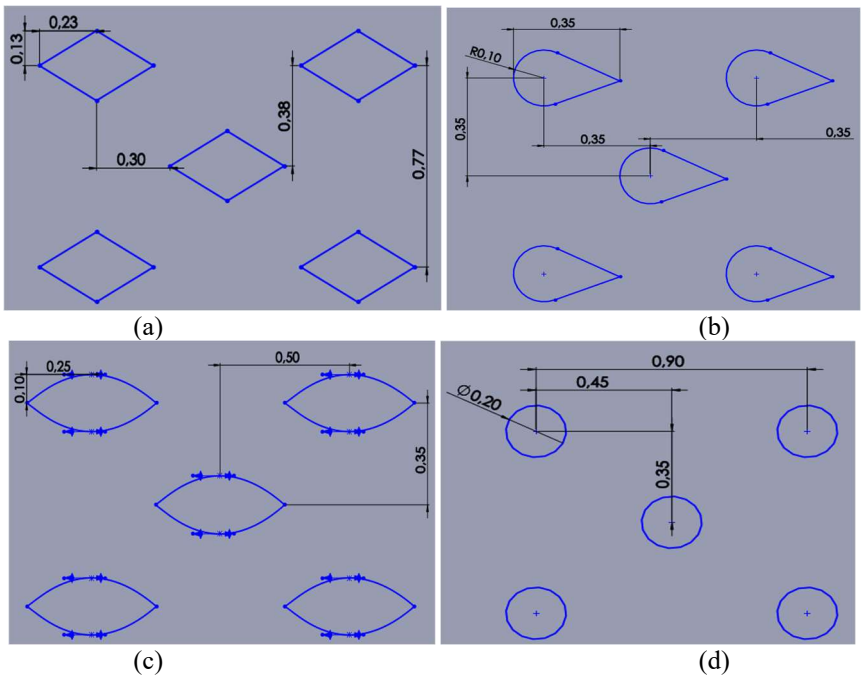

Figure 1. Proposed geometries: (a) diamond, (b) drop, (c) sinusoidal, (d) circle

Figure 2 shows photographs of the CrCoW alloy printed selected geometries (Mlab200R printer), besides four open geometries to enable the geometric evaluation of each type of heatsink in a more accessible way.

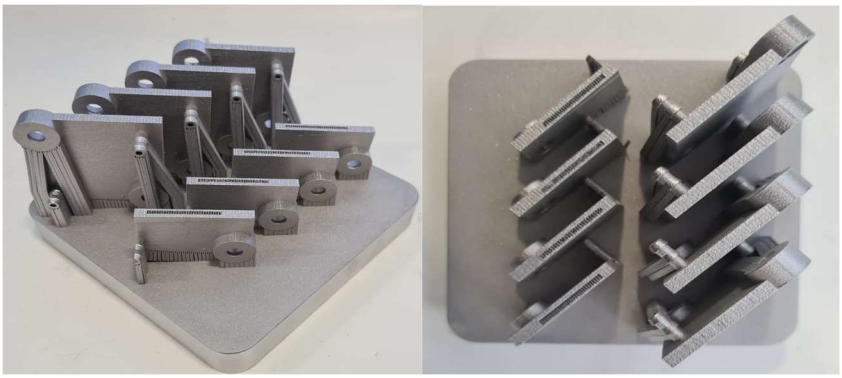

Figure 2. Final and open micro heat sinks geometries produced through DLMS (Mlab200R printer).

2. COMPUTATIONAL MODELLING

For fair comparisons of the results obtained numerically for the different proposed microchannel heat sinks, the heating system of the laboratory test bench was modelled in the CFD platform and the simulations were implemented.

Fig. 3 shows the summary of the regions and boundary conditions to be simulated, whose values were taken from one of the operating points evaluated experimentally. Likewise, in Tab. 1 the physical properties of each region are presented.

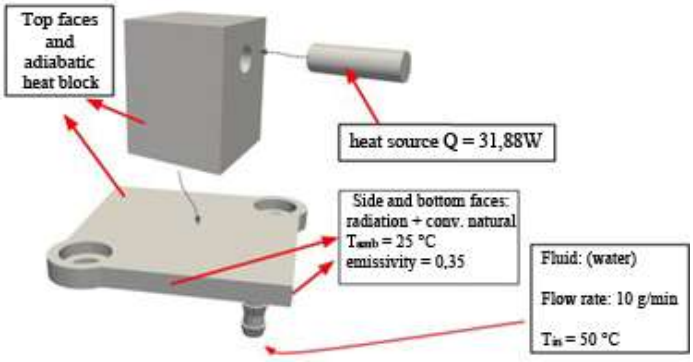

Figure 3. Regions and operating boundary conditions implemented in the simulation.

Table 1. Physical Properties of the solid regions of the heater/sink assembly.

Region	Thermal conductivity [W/(m.K)]	Density [kg/m³]	Specific heat [J/kg.K]
Heating resistance	60	8960	385
Aluminum base	138	2700	893
Micro heat sink	14.82	8387	422

For the solid regions of the simulation, listed in Tab. 1, we only have heat transfer by conduction, characterized by the following steady-state energy conservation equation:

$$\nabla \cdot \left[-\frac{k}{c_p} \nabla H \right] = \dot{q} \tag{1}$$

where k is the thermal conductivity of each material (W/m.K), c_p is the specific heat of the material at constant pressure (J/kg.K), H is the enthalpy (J/kg, such that $H = c_p T$) and $\dot{q}$ is the volumetric heat source [W/m^3]. For the heating resistor, total heat source is equal to $\dot{Q} = \dot{q}V = 31.88$ W, while in the other solids it is equal to zero.

Thus, at the interface of each solid, the heat is received from a neighboring region and dissipated to the next region by conduction. In the external walls of the solids, the boundary conditions are related to heat fluxes to the environment, q''_{wall}, given by the sum of the contributions of the natural convection (q''_{conv}) and radiation (q''_{rad}) in each exposed surface:

$$q''_{wall} = h\,(T_s - T_{amb}) + \varepsilon\,\sigma\,(T_s^4 - T_{amb}^4) \tag{2}$$

Where,

$$h = \begin{cases} \left.\begin{array}{l} 0.54\,\frac{k_{air}}{L_s}\,Ra^{\frac{1}{4}}\ ,\ 10^4 \le Ra \le 10^7 \\ 0.15\,\frac{k_{air}}{L_s}\,Ra^{\frac{1}{3}}\ ,\ 10^7 \le Ra \le 10^{11} \end{array}\right\}: \text{ hot upward surface} \\ 0.27\,\frac{k_{air}}{L_s}\,Ra^{0.25}\ ,\ 10^5 \le Ra \le 10^{11}: \text{ hot downward surface} \\ \left.\begin{array}{l} 0.59\,\frac{k_{air}}{L_s}\,Ra^{\frac{1}{4}}\ ,\ 10^4 \le Ra \le 10^9 \\ 0.10\,\frac{k_{air}}{L_s}\,Ra^{\frac{1}{3}}\ ,\ 10^9 \le Ra \le 10^{13} \end{array}\right\}: \text{ hot vertical surface} \end{cases} \tag{3}$$

$$Ra = \frac{g\,\beta_{air}\,L_s^3\,(T_s - T_{amb})}{\nu_{air}\,\alpha_{air}}, \quad L_s = \frac{A}{P}, \quad \beta_{air} = \frac{1}{T_f}, \quad T_f = \frac{T_s + T_{amb}}{2} \tag{4-7}$$

h is the convective heat transfer coefficient, Ra is the Rayleigh number, g is the acceleration of gravity, and α_{air} $(= k_{air}/(\rho_{air} c_{pair}))$, ν_{air} $(= \mu_{air}/\rho_{air})$, and β_{air}, are the thermal diffusivity, the kinematic viscosity and the volumetric expansion coefficient of the air, respectively. L_s is the characteristic plate length, given by the ratio between the plate

surface area (A) and its perimeter (P). T_s and T_{amb} are the surface and environment temperatures. The thermodynamic properties of air as a function of temperature (in Kelvin) are shown in Tab. 2. In the radiation calculations, ε is the emissivity of the material ($\varepsilon = 0.35$ for CoCrW alloy) and σ is the Stefan-Boltzmann constant ($\sigma = 5.67 \times 10^{-8}$ W/m^{2}K^4).

Table 2. Temperature dependence of the thermo-physical properties of air.

Property	Polynomial fit (film temperature dependence)
k [W/m.K]	$10^{-3}\times\left(2.5219 + 8.506\times10^{-2}T_f - 1.312\times10^{-5}T_f^2\right)$
ρ [kg/m^3]	$2.0132 - 0.0034\,T_f$
μ [kg/m.s]	$10^{-6}\times\left(1.5061 + 6.16\times10^{-2}T_f - 1.819\times10^{-5}T_f^2\right)$
c_p [J/kg.K]	$948.76 + 0.39171\,T_f - 10^{-4}\times\left(9.5999\,T_f^2 - 1.393\times10^{-2}T_f^3 + 6.2029\times10^{-6}T_f^4\right)$

The simulations performed in the present work were conducted in OpenFOAM, an open-source software for computational fluid dynamics simulations, based on the FVM (Jasak, 1996). Specifically for the heat sink problem, the multiregion solver *chtMultiRegionSimpleFoam* was used, which simultaneously solves the transport equations of multiple solid and fluid regions, in steady state, allowing the coupling between these regions through boundary conditions called interface conditions. At these interfaces, the boundary values of the boundary of a region are mapped to the boundary with which it interacts, and a relationship of the same property value can be established between these two boundaries (as is generally the case for temperatures) and property flow relationships between one region and another.

Besides the dimensions presented in Fig. 1, Table 3 brings additional information about the main geometric characteristics of pin fin heatsinks simulated. Additionally, since comparisons will be performed with a microchannel heat sink of rectangular straight geometry its characteristics are also listed in this table.

Table 3. Main geometric parameters of pin fin heat exchangers.

				Micro pin-fin geometry			
Description	**Variable**	**Unit**	**Straight Microchannel**	**Circle**	**Drop**	**Sine**	**Diamond**
Cross-sectional area	A_{st}	[mm^2]	4.58[a]	0.03[b]	0.04[b]	0.07[b]	0.06[b]
Pin height (channel height)	H	[mm]	1.0	1.5	1.5	1.5	1.5
Length of the heat sink	L	[mm]	22.88	22.88	22.88	22.88	22.88
Number of pins (microchannels)	N	[-]	53	1534	1918	1357	1161
Heat exchange (wet) area	A_w	[mm^2]	2628.8	1514.4	2542.86	2307.69	1932.04
Total volume of pin fins (solid)	V_{tot}	mm^3	242.53	69.03	115.08	142.49	104.49

a - Cross-sectional area (top view) of one microchannel wall b - Cross-sectional area (top view) of one single pin fin

The values of the operational parameters considered in the simulations for all heat exchangers are summarized in Tab. 4. Since the surface temperature, T_s, is not known at priori, an iterative procedure for evaluation of the boundary conditions that depends on this variable is implemented. Besides, once the experimental setup can't be considered perfectly insulated, an additional 10% heat loss, based on experimental measurements, is adopted in the simulations.

Table 4 - Operating conditions implemented in the simulations.

Operating condition	Variable	Unit	Value
Heat source power	Q	[W]	31.88
Environment temperature	T_{amb}	[°C]	25
Convective heat transfer coefficient	h	[W/m^{2}K]	Eq. (3)
Coolant fluid volumetric flow rate	$\dot{V}$	[ml/min]	10, 20, 30
Coolant fluid inlet temperature	T_{in}	[°C]	50

3. RESULTS

A mesh converge analysis is performed for the microchannel heat sink straight channel with rectangular cross section geometry, the simplest geometry that will be employed for comparison purposes. Three meshes were used to verify the energy balance between the different regions of the computational domains, as well as the micro heat sink outlet temperature of the coolant fluid. These meshes are named M1 (4.89 x 10^6 elements), M2 (9.62 x 10^6 elements), and M3 (13.17 x 10^6 elements), and are illustrated in Table 5, where the mesh clustering characteristic near the interface regions of each computational domain is highlighted.

Since the computational domain is of multi-region type, the heat transfer rate at the domains interfaces between each region (cartridge resistance, heating block, heat sink and coolant fluid) is employed as the convergency parameter, as illustrated in Table 6. From this table, it is possible to see that the results for the heat transfer rate can only be considered converged for the M3 mesh, since it is the mesh that minimizes the differences between heat transmitted and received between the regions. This behavior shows that for the pin-fin micro heat sinks the mesh should have a number of elements of the same order of mesh M3, at least.

After this preliminary mesh convergence, the selected pin-fin heat sink geometries were analyzed by following the same methodology applied to the microchannel heat sink studied. The number of mesh elements employed in each case (circle, drop, sinusoidal and diamond) is described in Table 7. It is worth to mention that due to the sharp edges of the pin-fin with diamond shape, a mesh with the double of elements of mesh M3 is required for good convergence. The general aspects and details of the meshes of the fluid region for each geometry are also illustrated in Table 7.

Table 5. Mesh characteristics of each region of the computational domain.

Region	**Mesh characteristics**		
	M1 (4.89×10^6 elements)	**M2** (9.62×10^6 elements)	**M3** (13.17×10^6 elements)
Cartridge resistance	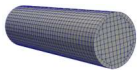	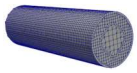	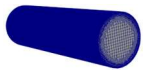
Heating block		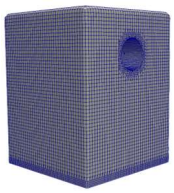	
Heat sink solid region	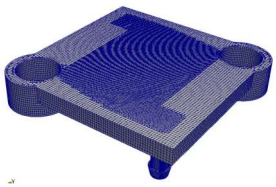	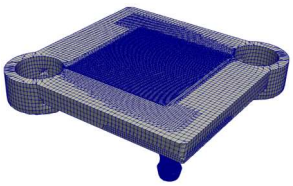	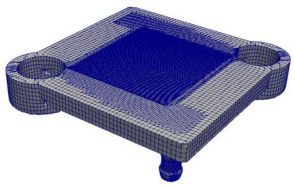
Heat sink fluid region	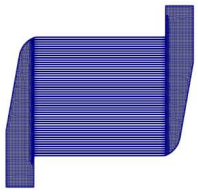	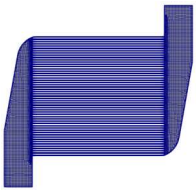	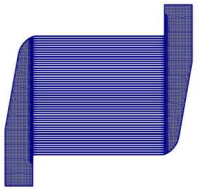

Table 6. Mesh convergence for the heat transfer rate between each computational domain.

Region	**Heat transfer at the interfaces**	**Mesh**		
		M1	**M2**	**M3**
		Heat Transfer Rate - Q [W]		
Cartridge resistance	Transmitted to the heating block	-31.88	-31.88	-31.89
Heating block	Received from the cartridge resistance	31.71	31.94	31.76
	Dissipated to the environment	0	0	0
	Transmitted to the heat sink	-31.71	-31.94	-31.80
Heat sink solid region	Received from the heating block	27.11	30.73	31.84
	Dissipated to the environment	-3.51	-3.41	-3.42
	Transmitted to the heat sink fluid	-23.59	-27.73	-28.62
Heat sink fluid region	Received from the heat sink	21.52	27.74	28.61

The mesh convergence analysis from the energy balance between the regions of the different computational domains was also verified for the pin-fin micro heat sinks. Here, the maximum, average and minimum deviations of heat transferred between the regions are presented in Table 8. From this table, it is clear that the number of elements implemented in the mesh of each one of the evaluated pin heat sinks is adequate.

Table 7. Mesh detail of the fluid region of the pin-fin micro heat sink

Pin-fin geometry			
Circle (12.80×10^6 elements)	Drop (13.32×10^6 elements)	Sinusoidal (13.38×10^6 elements)	Diamond (25.18×10^6 elements)
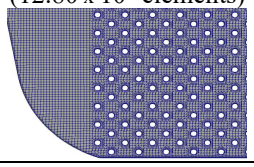	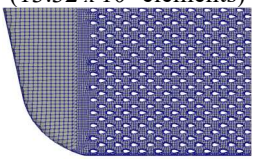	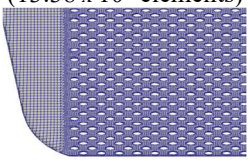	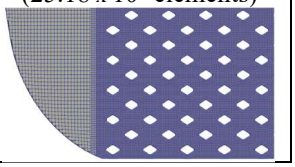

Table 8. Heat transfer rate deviations for the different pin-fin geometries for the meshes employed.

Deviation [%]	**Pin-fin geometry**			
	Circle	**Drop**	**Sine**	**Diamond**
Maximum	1.92	1.22	1.22	0.57
Medium	0.87	1.10	0.62	0.39
Minimum	0.16	0.89	0.03	0.11

Now, results for the friction factor (f) and the local heat transfer coefficient (h) are analyzed for different volumetric flow rates (10, 20 and 30 ml/min). Here, these parameters ae evaluated according to the approach described in Kewalramani et al. (2019). The overall friction factor is based on the Darcy equation, being a function of the heat sink pressure drop (Δp), length (L), hydraulic diameter (d_h), and fluid mean velocity (u) and density (ρ):

$$f = \frac{2\,\Delta p\,d_h}{\rho\,L\,u^2} \tag{10}$$

For this kind of geometry, Haaksman et al. (2017) proposes to evaluate hydraulic diameter as function of the ratio between the total volume of pin fins (V_{tot}) and the wall surface areas (pin fins, A_{pins}, and channel walls, A_{wall}):

$$d_h = \frac{4\,V_{tot}}{A_{wall} + A_{pins}} \tag{11}$$

Therefore, taking a line along the micro heat sink, the local friction factor can be defined as (where $p(x)$, $u(x)$, $\rho(x)$ are the local flow pressure, axial velocity and density along the line, and p_{exit} is the pressure at the exit of the heat sink):

$$f(x) = \frac{2\,[p(x) - p_{exit}]\,d_h}{\rho(x)\,L\,u(x)^2} \tag{12}$$

Similarly, the local convective heat transfer coefficient along the same straight line, $h(x)$, is evaluated as function of the heat flux (q''), and the local and mean micro heat sink temperatures ($T(x)$, T_m):

$$h(x) = \frac{q''}{[T(x) - T_m]} \tag{12}$$

Figure 4 shows the behavior of the local friction factor along the micro heat sink length at its symmetry line, for the three flow rates analyzed. This figure reveals that the local friction factor for the micro heat sink with diamond pin fins (Fig. 4c) is the highest of all geometries. This behavior is due to sharp vertices present in this geometry and that strongly impair the flow dynamics. For the other formats, the friction factor varies similarly and, thus, it can be concluded that the hydrodynamic characteristics of the heat sink with the pin fins with circular, drop, and sinusoidal shapes are similar.

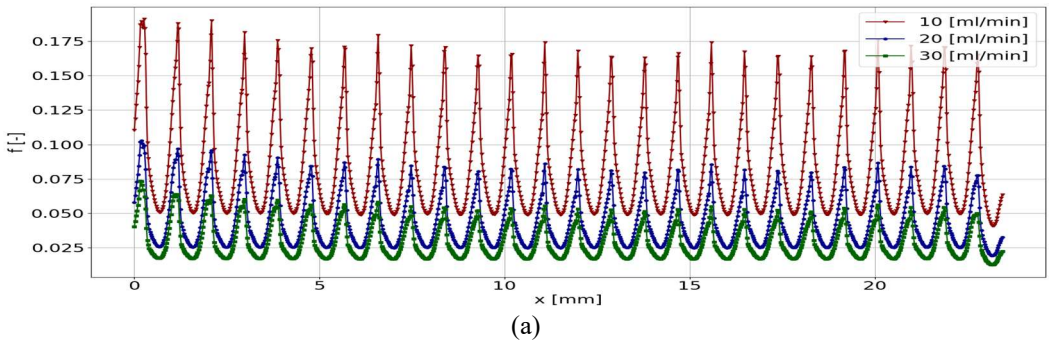

(a)

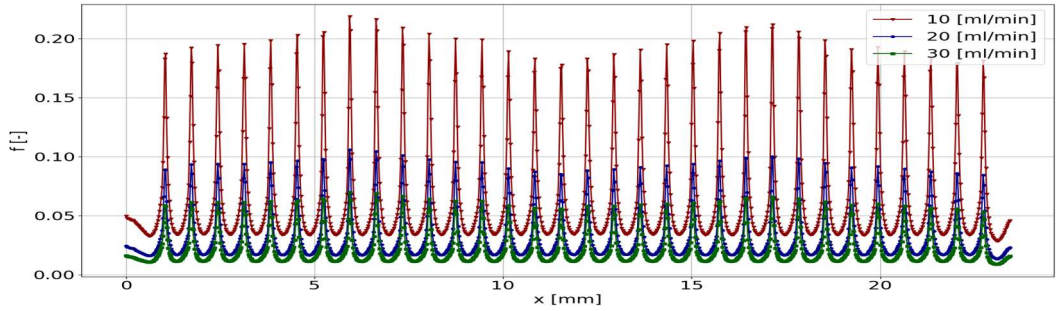

(b)

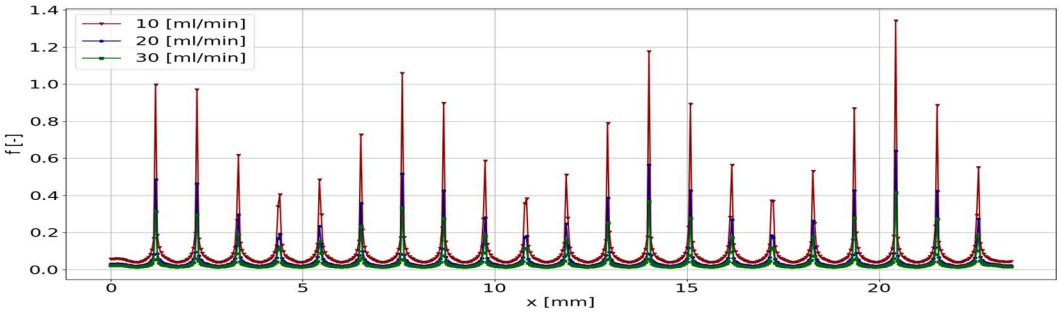

(c)

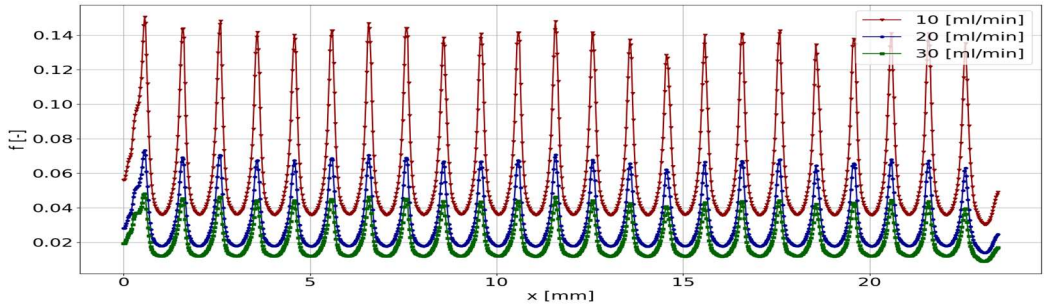

(d)

Figure 4. Friction factor along the pin-fin heat sink: a) Circular, b) Drop, c) Diamond and d) Sinusoidal

Figure 5 shows the variation in the local heat transfer coefficient in a central position of domain around different rows of fins for the different flow rates. The pin-fin rows where the main variations of *h* occur are shown, identified with the respective numbers above. It can be seen that the heat transfer coefficient is maximum in a region between the central part and the outlet (x ≅ 16 mm) of the heat sink, and as the flow passes through each row of pins, the local heat transfer coefficient varies less around the pin fin. It can also be noted that as the inlet flow rate increases, the average value of the local heat transfer coefficient around the pins also increases due to the increase in the size of the vortex around a pin.

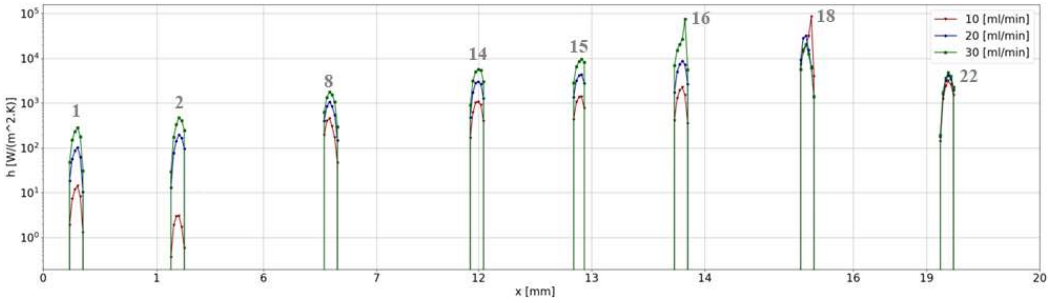

(a)

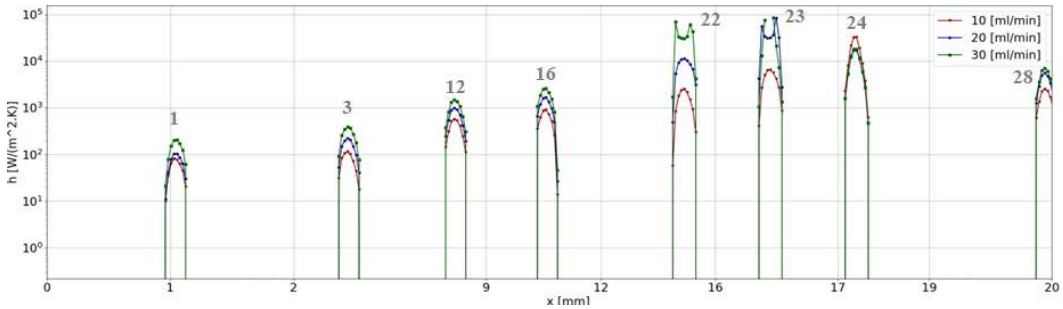

(b)

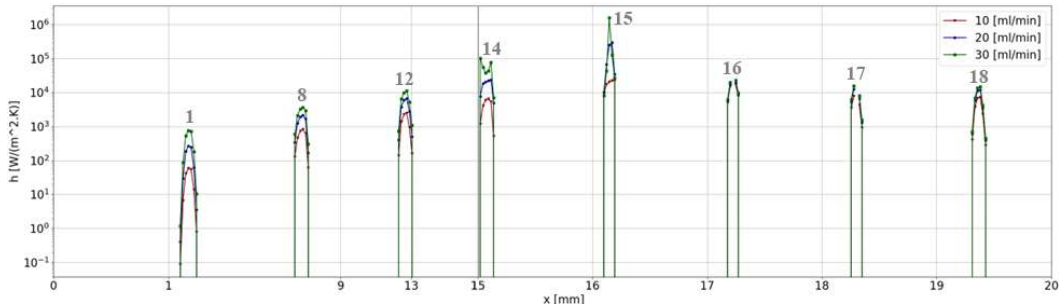

(c)

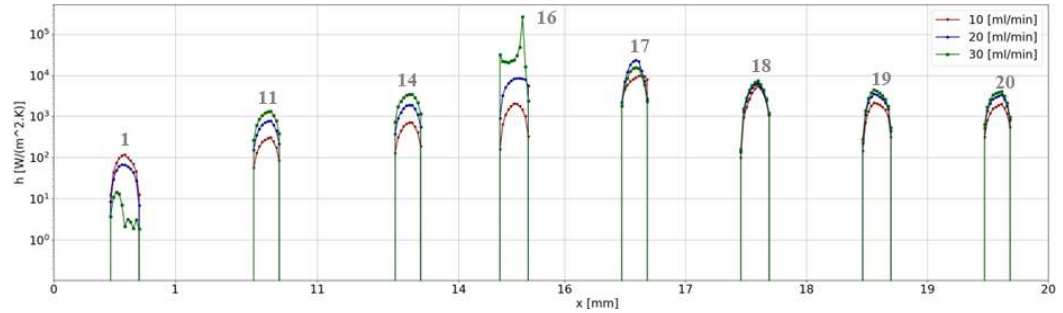

(d)

Figure 5. Heat transfer coefficient along the pin-fin heat sink: a) Circular, b) Drop, c) Diamond and d) Sinusoidal

The results for the pressure drop, fluid outlet (T_{out}) temperature and heat sink mean surface temperature (T_{surf}) obtained with the present simulations are presented in Tab. 9 for the pin-analyzed pin-fin geometries and for the straight microchannel heat sink. Comparing the results between the microchannel and the pin-fin heat sinks, it is concluded that the pin-fin heat sinks present the best compromise between pressure drop (smaller) and thermal performance (higher).

Table 9. Pressure drop, fluid outlet temperature and heat sink mean surface temperatures for each micro heat sinks. Volumetric flow rate of 10 ml/min.

Output	**Straight microchannel**	**Pin-fin geometry**			
		Circle	**Drop**	**Sinusoidal**	**Diamond**
ΔP [Pa]	153	33.89	40.46	33.85	30.03
T_{out} [ºC]	88.90	88.02	93.00	92.12	91.12
T_{surf} [ºC]	85.66	85.80	91.30	89.19	86.03

From the average outlet temperature obtained for the case of the drop heat sink, of 93.00 ºC, it is possible to state that the use of this type of pin fin as a geometry for thermal exchanges proved to be more efficient than all the heat sinks evaluated. Abdoli et al. (2015) numerically investigated the influence of different pin fins (circular, droplet, sinusoidal) for cooling electronic chips and obtained the droplet shape as the best thermal performance. İzci et al. (2015) obtained the highest heat transfer coefficient for the drop shape, followed by the square shape. It was observed that pin fins with protruding corners have this thermal performance in relation to more simplified geometries.

The average outlet temperature for the sinusoidal geometry is 92.12 °C. Here it is also possible to state that the use of sine-type pin fins promotes greater heat transfer to the fluid. Zhao et al. (2016) experimentally showed that sine-shaped geometry has better flow line with low thermal resistance and the triangle-shaped geometry has higher flow resistance

compared to other shapes. In Yang et al. (2017), who used an inlet flow of 100 mL/min, this geometry was the one that obtained the best performance, unlike the present research in which it ended up being relatively inferior to the drop shape.

The average temperature of the fluid outlet for the diamond geometry reached only 91.12 ºC. This geometry is characterized in some literature as the one with the lowest pressure drop (Ambreen et al., 2022; Yang et al., 2017), but its thermal performance is below the droplet geometry. For a global view of the thermal behavior of the heat sink designs, Figure 6 shows the temperature fields of the fluid region for each pin-fin heatsinks. It is observed that the top of the aluminum base reaches temperatures of up to 104 ºC in most cases simulated with pins.

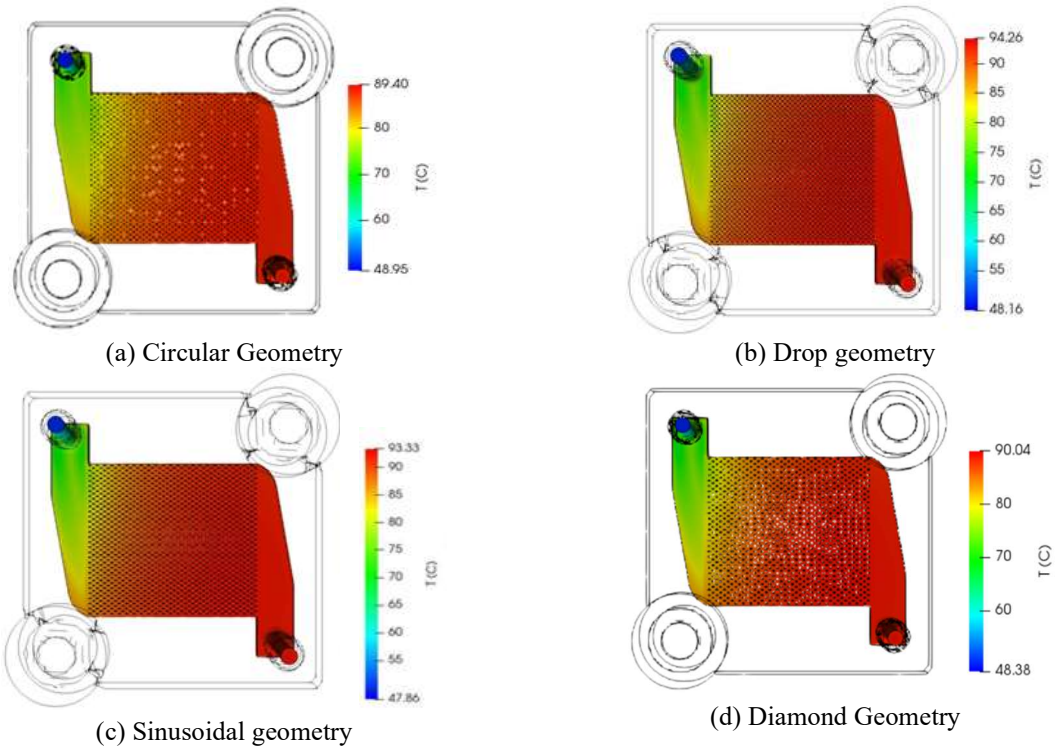

(a) Circular Geometry

(b) Drop geometry

(c) Sinusoidal geometry

(d) Diamond Geometry

Figure 6. Temperature field of the fluid regions of the pin heatsinks.

4. CONCLUSION

In general, the numerical simulations were able reproduce the general behavior expected in the literature for cases with pin fins, considering all heat losses to the surroundings. The proposed CFD modeling, therefore, proved to be effective for this type of analysis. The construction of channels with pin fins proved to be effective in terms of heat exchange, where it can be seen that they present a significant relationship with a smaller pressure drop and a higher thermal performance, comparing the simulated results between the microchannel and the pin-fin heat sinks. The droplet model produced the highest heat exchanges, for providing the highest outlet temperature and for having the largest heat exchange area among the others and, despite having the highest pressure drop, resulted in the highest enthalpy gain by the fluid at the exit of the HCPV exchanger. In its geometric form, in the use of pin fins, it could be observed that use of irregular and not so usual shapes led to better results, due to the modification of the flow dynamics caused by this fact.

The results obtained were relevant in order to maximize the use of heat rejected by the photovoltaic cells. As next steps, tests will be carried out on the bench and, later, on the HCPV panel to validate the results obtained with the new geometries. However, more simulations will be carried out from other operating points tested on the bench in order to have a greater number of comparable results to increase confidence in the implemented methodology.

5. ACKNOWLEDGEMENTS

Partial funding by Petrogal Brasil Project GALP/38, and the sponsoring agencies CNPq, FAPERJ, and CAPES/PROCAD Defesa, are gratefully acknowledged. P.R. Júnior acknowledges the engineers Natalia C. de Sá, Eduardo P. dos Santos and Filipe E. Cunha de Souza for their help in the execution of the computational code developed.

6. REFERENCES

Abdoli, A., Jimenez, G., & Dulikravich, G. S. (2015). Thermo-fluid analysis of micro pin-fin array cooling configurations for high heat fluxes with a hot spot. *International Journal of Thermal Sciences*, *90*, 290–297. https://doi.org/10.1016/j.ijthermalsci.2014.12.021

AlFalah, G., Maatallah, T. S., Okasha, A. T., & Al-Amri, F. G. (2022). Design and optimization study of a densely packed ultrahigh concentration photovoltaic thermal array for desalination usability. *International Journal of Energy Research*, *46*(2), 1693–1710. https://doi.org/10.1002/er.7285

Ali, H. M., & Arshad, W. (2015). Thermal performance investigation of staggered and inline pin fin heat sinks using water based rutile and anatase TiO2 nanofluids. *Energy Conversion and Management*, *106*, 793–803. https://doi.org/10.1016/J.ENCONMAN.2015.10.015

Ambreen, T., Saleem, A., Tanveer, M., K, A., Shehzad, S. A., & Park, C. W. (2022). Irreversibility and hydrothermal analysis of the MWCNTs/GNPs-based nanofluids for electronics cooling applications of the pin-fin heat sinks: Multiphase Eulerian-Lagrangian modeling. *Case Studies in Thermal Engineering*, *31*(December 2021), 101806. https://doi.org/10.1016/j.csite.2022.101806

Baisar, M., & Briggs, A. (2009). Condensation of Steam on Pin-Fin Tubes: Effect of Circumferential Pin Thickness and Spacing. *Heat Transfer Engineering*, *30*(13), 1017–1023. https://doi.org/10.1080/01457630902921014

Cohen, J., & Bourell, D. L. (2016). Development of novel tapered pin fin geometries for additive manufacturing of compact heat exchangers. *Solid Freeform Fabrication 2016: Proceedings of the 27th Annual International Solid Freeform Fabrication Symposium - An Additive Manufacturing Conference, SFF 2016*, 2314–2336.

Haaksman, V.A., Siddiqui, A., Schellenberg, C., Kidwell, J., Vrouwenvelder, J.S., Picioreanu, C. (2017). Characterization of feed channel spacer performance using geometries obtained by X-ray computed tomography. *Journal of Membrane Science,* 522, 124–139.

İzci, T., Koz, M., & Koşar, A. (2015). The Effect of Micro Pin-Fin Shape on Thermal and Hydraulic Performance of Micro Pin-Fin Heat Sinks. *Heat Transfer Engineering*, *36*(17), 1447–1457. https://doi.org/10.1080/01457632.2015.1010921

Jasak, H. (1996). *Error Analysis and Estimation for the Finite Volume Method with Applications to Fluid Flows*. Imperial College London (University of London).

Kewalramani., G.V., Hedau, G., Saha, S.K., Agrawal, A. (2019). Study of laminar single phase frictional factor and Nusselt number in In-line micro pin-fin heat sink for electronic cooling applications. *International Journal of Heat and Mass Transfer*, 138, 796-808.

Klein, E., Ling, J., Aute, V., Hwang, Y., & Radermacher, R. (2018). A Review of Recent Advances in Additively Manufactured Heat Exchangers. *International Refrigeration and Air Conditioning Conference*, *2006*, 1–10. https://docs.lib.purdue.edu/iracc%0Ahttps://docs.lib.purdue.edu/iracc/1983

Mohammadi, A., & Koşar, A. (2019). The effect of arrangement type and pitch ratio on the performance of micro-pin-fin heat sinks. *Journal of Thermal Analysis and Calorimetry 2019 140:3*, *140*(3), 1057–1068. https://doi.org/10.1007/S10973-019-08840-2

Morrison, D. G. (2002). Heatsinks Shape Up To Face New Thermal Challenges. *Computers & Applied Sciences Complete Academic Search Premier*, *50*(23), 55.

Radmard, V., Hadad, Y., Rangarajan, S., Hoang, C. H., Fallahtafti, N., Arvin, C. L., Sikka, K., Schiffres, S. N., & Sammakia, B. G. (2021). Multi-objective optimization of a chip-attached micro pin fin liquid cooling system. *Applied Thermal Engineering*, *195*, 117187. https://doi.org/10.1016/J.APPLTHERMALENG.2021.117187

Roth, R., Lenk, G., Cobry, K., & Woias, P. (2013). Heat transfer in freestanding microchannels with in-line and staggered pin fin structures with clearance. *International Journal of Heat and Mass Transfer*, *67*, 1–15. https://doi.org/10.1016/J.IJHEATMASSTRANSFER.2013.07.097

Tang, J., Li, X., Hu, R., Mo, Z., & Du, M. (2022). A novel designed manifold ultrathin micro pin-fin channel for thermal management of high-concentrator photovoltaic system. *International Journal of Heat and Mass Transfer*, *183*, 122094. https://doi.org/10.1016/j.ijheatmasstransfer.2021.122094

Tsopanos, S., Wong, M., Owen, I., & Sutcliffe, C. J. (2006). *Manufacturing Novel Heat Transfer Devices By Selective Laser Melting*. 13–18. https://doi.org/10.1615/ihtc13.p13.40

Wang, A. C., Yan, B. H., Tang, Y. X., & Huang, F. Y. (2005). The feasibility study on a fabricated micro slit die using micro EDM. *International Journal of Advanced Manufacturing Technology*, *25*(1–2), 10–16. https://doi.org/10.1007/s00170-003-1831-7

Yan, Y., Zhao, T., He, Z., Yang, Z., & Zhang, L. (2021). Numerical investigation on the characteristics of flow and heat transfer enhancement by micro pin-fin array heat sink with fin-shaped strips. *Chemical Engineering and Processing - Process Intensification*, *160*, 108273. https://doi.org/10.1016/J.CEP.2020.108273

Yang, D., Jin, Z., Wang, Y., Ding, G., & Wang, G. (2017). Heat removal capacity of laminar coolant flow in a micro channel heat sink with different pin fins. *International Journal of Heat and Mass Transfer*, *113*, 366–372. https://doi.org/10.1016/j.ijheatmasstransfer.2017.05.106

Zhao, H., Liu, Z., Zhang, C., Guan, N., & Zhao, H. (2016). Pressure drop and friction factor of a rectangular channel with staggered mini pin fins of different shapes. *Experimental Thermal and Fluid Science*, *71*, 57–69. https://doi.org/10.1016/j.expthermflusci.2015.10.010

7. RESPONSIBILITY NOTICE

The authors are the only responsible for the printed material included in this paper.